

Convergence of High Order Finite Volume Weighted Essentially Non-Oscillatory Scheme and Discontinuous Galerkin Method for Nonconvex Conservation Laws¹

Jing-Mei Qiu² and Chi-Wang Shu³

Division of Applied Mathematics, Brown University, Providence, Rhode Island 02912

Abstract

In this paper, we consider the issue of convergence toward entropy solutions for high order finite volume weighted essentially non-oscillatory (WENO) scheme and discontinuous Galerkin (DG) finite element method approximating scalar nonconvex conservation laws. Although such high order nonlinearly stable schemes can usually converge to entropy solutions of convex conservation laws, convergence may fail for certain nonconvex conservation laws. We perform a detailed study to demonstrate such convergence issues for a few representative examples, and suggest a modification of the high order schemes based either on first order monotone schemes or a second order entropic projection [1] to achieve convergence toward entropy solutions while maintaining high order accuracy in smooth regions.

Keywords: nonconvex conservation laws; discontinuous Galerkin method; finite volume WENO scheme; convergence; entropy solution; entropic projection

¹Research supported by ARO grant W911NF-04-1-0291, NSF grant DMS-0510345 and AFOSR grant FA9550-05-1-0123.

²E-mail: jqi@dam.brown.edu

³E-mail: shu@dam.brown.edu

Report Documentation Page			Form Approved OMB No. 0704-0188		
Public reporting burden for the collection of information is estimated to average 1 hour per response, including the time for reviewing instructions, searching existing data sources, gathering and maintaining the data needed, and completing and reviewing the collection of information. Send comments regarding this burden estimate or any other aspect of this collection of information, including suggestions for reducing this burden, to Washington Headquarters Services, Directorate for Information Operations and Reports, 1215 Jefferson Davis Highway, Suite 1204, Arlington VA 22202-4302. Respondents should be aware that notwithstanding any other provision of law, no person shall be subject to a penalty for failing to comply with a collection of information if it does not display a currently valid OMB control number.					
1. REPORT DATE 2007		2. REPORT TYPE		3. DATES COVERED 00-00-2007 to 00-00-2007	
4. TITLE AND SUBTITLE Convergence of High Order Finite Volume Weighted Essentially Non-Oscillatory Scheme and Discontinuous Galerkin Method for Nonconvex Conservation Laws				5a. CONTRACT NUMBER	
				5b. GRANT NUMBER	
				5c. PROGRAM ELEMENT NUMBER	
6. AUTHOR(S)				5d. PROJECT NUMBER	
				5e. TASK NUMBER	
				5f. WORK UNIT NUMBER	
7. PERFORMING ORGANIZATION NAME(S) AND ADDRESS(ES) Brown University,Division of Applied Mathematics,Providence,RI,02912				8. PERFORMING ORGANIZATION REPORT NUMBER	
9. SPONSORING/MONITORING AGENCY NAME(S) AND ADDRESS(ES)				10. SPONSOR/MONITOR'S ACRONYM(S)	
				11. SPONSOR/MONITOR'S REPORT NUMBER(S)	
12. DISTRIBUTION/AVAILABILITY STATEMENT Approved for public release; distribution unlimited					
13. SUPPLEMENTARY NOTES					
14. ABSTRACT					
15. SUBJECT TERMS					
16. SECURITY CLASSIFICATION OF:			17. LIMITATION OF ABSTRACT	18. NUMBER OF PAGES 40	19a. NAME OF RESPONSIBLE PERSON
a. REPORT unclassified	b. ABSTRACT unclassified	c. THIS PAGE unclassified			

1 Introduction

In this paper, we consider the Cauchy problem of one dimensional scalar conservation laws:

$$\begin{cases} u_t + f(u)_x = 0, & \text{in } \mathbb{R} \times [0, T], \\ u(x, 0) = u_0(x), & \text{in } \mathbb{R}. \end{cases} \quad (1.1)$$

The unique entropy solution of (1.1) satisfies

$$U(u)_t + F(u)_x \leq 0 \quad (1.2)$$

in the distribution sense, for any convex entropy function $U(u)$ and its corresponding entropy flux function $F(u)$ satisfying $F'(u) = U'(u)f'(u)$.

If (1.1) is a convex (or concave) conservation law, that is, if $f''(u)$ does not change sign, we would only need the entropy condition (1.2) to be satisfied for one strictly convex entropy in order to determine the unique entropy solution of (1.1). When (1.1) is non-convex, namely when $f''(u)$ changes sign, the solution structure of (1.1) is much more complicated. This can already be seen from the simple Riemann problem with the initial condition

$$u_0(x) = \begin{cases} u_l, & \text{for } x < 0, \\ u_r, & \text{for } x \geq 0. \end{cases} \quad (1.3)$$

The discontinuity at the origin generates a single shock or a rarefaction wave for a convex conservation law, while for nonconvex conservation laws, much more complicated solution structures, sometimes called a compound wave, might be generated. The compound wave involves a sequence of shocks and rarefaction waves and is much harder to be resolved numerically. The entropy solution of the nonconvex Riemann problem can be determined from a convex-hull construction [8].

Numerical methods for nonlinear hyperbolic equations are expected to be able to efficiently capture the unique entropy solution. It is well known that first order monotone schemes converge to entropy solutions of both convex and nonconvex conservation laws [3], but with a relatively slow convergence rate. For high order numerical methods, for example the high order finite difference or finite volume WENO schemes [9, 6, 13] and discontinuous

Galerkin method [2], however, very few theoretical results on convergence are available for discontinuous solutions.

The high order finite volume WENO scheme, about which we provide a brief review in section 2.1, is one of the successful high order numerical methods in approximating (1.1). Based on the idea of adaptive stencils in the reconstruction procedure, WENO schemes would automatically achieve high order accuracy in smooth regions of the solution and an essentially non-oscillatory resolution at the discontinuities. Despite its good numerical performance in many applications, the theoretical proof for its convergence towards the entropy solution is very difficult. Typically, one would need a cell entropy inequality [10], or a wavewise entropy inequality [17], together with the total variation bounded (TVB) property of the numerical solutions to imply such convergence. There are counter examples for nonconvex conservation laws [18], such that high order Godunov schemes would not be able to converge to the entropy solution under the usual time step governed by the CFL condition. For the Godunov schemes under large time steps, convergence is available with up to third order reconstruction operators [11]. Though this convergence result holds for both convex and nonconvex conservation laws in multiple space dimensions, the implementation of the scheme for nonconvex conservation laws and for multiple space dimensions is highly non-trivial.

The discontinuous Galerkin (DG) method is another class of high order numerical methods in approximating (1.1), about which we provide a brief review in section 2.2. It is a finite element method, but uses discontinuous, typically piecewise polynomial functions to form the solution and test spaces, and adopts finite volume techniques including numerical fluxes and limiters. It can be proved that the semi-discrete DG method satisfies a cell entropy inequality for the square entropy [5], which implies convergence to the unique entropy solution for one dimensional scalar convex conservation laws if it converges. For nonconvex conservation laws, an entropy inequality for a single entropy is not enough to imply convergence to the entropy solution. Examples for which numerical solutions of the DG method fail to converge to the correct entropy solution for nonconvex conservation laws will be demonstrated

in section 3.

In this paper, we propose a first order monotone modification in the framework of high order finite volume WENO scheme and the discontinuous Galerkin method to enforce convergence towards the entropy solution. A discontinuity indicator is introduced to avoid the degeneracy of high order accuracy in smooth regions. Based on the idea of a MUSCL type scheme satisfying all the entropy inequalities in [1], a second order modification with an entropic projection is also proposed for high order numerical schemes.

This paper is organized as follows. Section 2 gives a brief review on high order finite volume WENO and discontinuous Galerkin methods. Section 3 demonstrates the performance of different numerical methods for nonconvex conservation laws through several examples. A first order monotone modification, as well as a second order modification with an entropic projection are proposed for high order numerical methods in section 4 and section 5 respectively. Numerical examples are shown to demonstrate the quality of proposed schemes. Concluding remarks are given in section 6.

2 High order numerical methods

In this section, we briefly review two classes of high order numerical schemes, i.e. the high order finite volume WENO scheme and the discontinuous Galerkin method in approximating (1.1). This forms the basis for our discussion in later sections on high order numerical methods. Throughout the paper, we will always use the following notation for the meshes unless otherwise specified. The computational interval is divided into N subintervals, each of which is denoted as a cell $I_j = [x_{j-\frac{1}{2}}, x_{j+\frac{1}{2}}]$ with the cell center $x_j = \frac{1}{2}(x_{j-\frac{1}{2}} + x_{j+\frac{1}{2}})$ and the cell length $\Delta x_j = (x_{j+\frac{1}{2}} - x_{j-\frac{1}{2}})$. We also denote the maximum cell size as $\Delta x = \max_j \Delta x_j$.

2.1 The finite volume WENO scheme

One of the successful high order numerical methods for (1.1) is the class of finite volume WENO method [9, 6, 13]. It approximates the integral version of (1.1) by

$$\frac{d\bar{u}_j}{dt} = -\frac{1}{\Delta x_j}(\hat{f}_{j+\frac{1}{2}} - \hat{f}_{j-\frac{1}{2}}), \quad j = 1, \dots, N \quad (2.1)$$

where \bar{u}_j is the approximation to the cell average of the solution over the cell I_j

$$\bar{u}_j = \frac{1}{\Delta x_j} \int_{I_j} u(x, t) dx,$$

and

$$\hat{f}_{j+\frac{1}{2}} = \hat{f}(u_{j+\frac{1}{2}}^-, u_{j+\frac{1}{2}}^+) \quad (2.2)$$

is a monotone numerical flux (non-decreasing in the first argument and non-increasing in the second argument) at the cell boundary $x_{j+\frac{1}{2}}$. Examples of monotone fluxes include the Godunov flux,

$$\hat{f}^G(a, b) = \begin{cases} \min_{\xi \in [a, b]} f(\xi), & \text{if } a < b, \\ \max_{\xi \in [b, a]} f(\xi), & \text{if } b \leq a, \end{cases} \quad (2.3)$$

which is the least dissipative among all monotone fluxes, and the Lax-Friedrichs flux,

$$\hat{f}^{LF}(a, b) = \frac{1}{2}(f(a) + f(b) - \alpha(b - a)), \quad \alpha = \max_u |f'(u)|. \quad (2.4)$$

In (2.2), $u_{j+\frac{1}{2}}^-$ and $u_{j+\frac{1}{2}}^+$ are the reconstructed values of the solution from neighboring cell averages to the left and right of the cell interface $x_{j+\frac{1}{2}}$. Examples of high order reconstructions include second order MUSCL reconstruction and fifth order WENO reconstruction.

- Second order MUSCL reconstruction [15].

The reconstructed point values for the second order MUSCL scheme are obtained by

$$u_{j+\frac{1}{2}}^- = \bar{u}_j + \frac{1}{2}s_j, \quad u_{j+\frac{1}{2}}^+ = \bar{u}_{j+1} - \frac{1}{2}s_{j+1}, \quad (2.5)$$

where $s_j = m(\bar{u}_{j+1} - \bar{u}_j, \bar{u}_j - \bar{u}_{j-1})$ with the usual definition of the *minmod* function m [4]

$$m(a, b) = \frac{1}{2}(\text{sign}(a) + \text{sign}(b)) \min(|a|, |b|).$$

- Fifth order WENO reconstruction [6, 13].

The reconstructed point value for the fifth order WENO scheme is obtained by

$$u_{j+1/2}^- = \omega_1 u_{j+1/2}^{(1)} + \omega_2 u_{j+1/2}^{(2)} + \omega_3 u_{j+1/2}^{(3)}, \quad (2.6)$$

where $u_{j+1/2}^{(m)}$ are the three third order reconstructions on three different stencils given by

$$\begin{aligned} u_{j+1/2}^{(1)} &= \frac{1}{3} \bar{u}_{j-2} - \frac{7}{6} \bar{u}_{j-1} + \frac{11}{6} \bar{u}_j, \\ u_{j+1/2}^{(2)} &= -\frac{1}{6} \bar{u}_{j-1} + \frac{5}{6} \bar{u}_j + \frac{1}{3} \bar{u}_{j+1}, \\ u_{j+1/2}^{(3)} &= \frac{1}{3} \bar{u}_j + \frac{5}{6} \bar{u}_{j+1} - \frac{1}{6} \bar{u}_{j+2}, \end{aligned}$$

and the nonlinear weights ω_m are given by

$$\omega_m = \frac{\tilde{\omega}_m}{\sum_{l=1}^3 \tilde{\omega}_l}, \quad \tilde{\omega}_l = \frac{\gamma_l}{(\varepsilon + \beta_l)^2},$$

with the linear weights γ_l given by

$$\gamma_1 = \frac{1}{10}, \quad \gamma_2 = \frac{3}{5}, \quad \gamma_3 = \frac{3}{10},$$

and the smoothness indicators β_l given by

$$\begin{aligned} \beta_1 &= \frac{13}{12} (\bar{u}_{j-2} - 2\bar{u}_{j-1} + \bar{u}_j)^2 + \frac{1}{4} (\bar{u}_{j-2} - 4\bar{u}_{j-1} + 3\bar{u}_j)^2 \\ \beta_2 &= \frac{13}{12} (\bar{u}_{j-1} - 2\bar{u}_j + \bar{u}_{j+1})^2 + \frac{1}{4} (\bar{u}_{j-1} - \bar{u}_{j+1})^2 \\ \beta_3 &= \frac{13}{12} (\bar{u}_j - 2\bar{u}_{j+1} + \bar{u}_{j+2})^2 + \frac{1}{4} (3\bar{u}_j - 4\bar{u}_{j+1} + \bar{u}_{j+2})^2. \end{aligned}$$

Here ε is a parameter to avoid the denominator to become 0 and is taken as 10^{-6} .

The reconstructed point value $u_{j+1/2}^+$ is obtained in a mirror symmetric fashion with respect to $x_{j+1/2}$ as that for $u_{j+1/2}^-$. For more details on the reconstruction procedure, we refer to [6, 13].

The high order Godunov type scheme (see, e.g. [18, 11] for the definition of this scheme that we are using) is a fully discretized version of the finite volume scheme (2.1). It consists of the following three stages to evolve the cell averages from \bar{u}^n at n -th time level to \bar{u}^{n+1} :

1. *Reconstruction*: obtain a high order piecewise polynomial reconstruction $u^n(x)$ whose cell averages agree with the given cell averages \bar{u}^n . We denote this reconstruction operator as $Re(\bar{u}^n)$. Second order MUSCL and fifth order WENO reconstructions as described above are typical examples of this reconstruction operator.
2. *Evolution*: evolve $u^n(x)$ by the conservation law (1.1) *exactly* for a time step Δt , to obtain a solution $\tilde{u}^{n+1}(x)$ which is in general *not* piecewise polynomial anymore. We denote this evolution operator as $S_{\Delta t}(u^n)$.
3. *Averaging*: average the function $\tilde{u}^{n+1}(x)$ to obtain the cell averages \bar{u}^{n+1} at time level $n + 1$. We denote this averaging operator as $A(\tilde{u}^{n+1})$.

The Godunov type scheme, using the notations introduced above, can be described abstractly as

$$\begin{cases} \bar{u}^0 = A(u_0) \\ \bar{u}^{n+1} = A \circ S_{\Delta t} \circ Re(\bar{u}^n), \end{cases} \quad n = 0, 1, \dots \quad (2.7)$$

We remark that the exact evolution step is difficult to implement, however we do not need all the information of this exactly evolved solution $\tilde{u}^{n+1}(x)$, but only its cell averages. Therefore, it is usually possible to implement such Godunov type schemes in an efficient fashion. We refer to [11] for more details.

2.2 The discontinuous Galerkin method

Another class of successful high order numerical methods for (1.1) is the discontinuous Galerkin method. The discontinuous Galerkin method is a finite element method using discontinuous piecewise polynomial functions

$$V_{\Delta x}^k = \{p : p|_{I_j} \in P^k(I_j), \quad j = 1, 2, \dots, N\}, \quad (2.8)$$

as the solution space and the test space, where $P^k(I_j)$ denotes the set of polynomials of degree $\leq k$ on cell I_j . If we adopt a local orthogonal basis over I_j , say $\{v_l^{(j)}(x), l = 0, 1, \dots, k\}$, then

the numerical solution $u^{\Delta x}(x, t) \in V_{\Delta x}^k$ can be written as

$$u^{\Delta x}(x, t) = \sum_{l=0}^k u_j^{(l)}(t) v_l^{(j)}(x) \quad \text{for } x \in I_j \quad (2.9)$$

with

$$u_j^{(l)}(t) = \frac{1}{a_l} \int_{I_j} u^{\Delta x}(x, t) v_l^{(j)}(x) dx, \quad l = 0, 1, 2, \dots, k, \quad (2.10)$$

where $a_l = \int_{I_j} (v_l^{(j)}(x))^2 dx$ are the normalization constants.

A semidiscrete DG method for solving (1.1) is obtained by multiplying (1.1) by a test function $v(x) \in V_{\Delta x}^k$, integrating over I_j , and integrating by parts. Specifically, the evolution of the degrees of freedom $u_j^{(l)}(t)$ in (2.9) by the DG method is achieved by

$$\frac{d}{dt} u_j^{(l)} + \frac{1}{a_l} \left(- \int_{I_j} f(u^{\Delta x}(x, t)) \frac{d}{dx} v_l^{(j)}(x) dx + \hat{f}_{j+\frac{1}{2}} v_l^{(j)}(x_{j+\frac{1}{2}}) - \hat{f}_{j-\frac{1}{2}} v_l^{(j)}(x_{j-\frac{1}{2}}) \right) = 0, \quad (2.11)$$

$l = 0, 1, \dots, k.$

Here, $\hat{f}_{j+\frac{1}{2}}$ is a monotone numerical flux defined by (2.2) with $u_{j+\frac{1}{2}}^-$ and $u_{j+\frac{1}{2}}^+$ being the left and right limits of the discontinuous solution $u^{\Delta x}$ at the cell interface $x_{j+\frac{1}{2}}$.

The DG method is a linear method, hence it cannot capture discontinuities without spurious oscillations when the order of accuracy is higher than one. Typically, nonlinear limiters similar to those used in high resolution finite volume schemes are used to suppress those oscillations. In this paper, we adopt the WENO limiter proposed in [12]. We refer to [12] for the details of the implementation of this WENO limiter.

2.3 Total variation diminishing (TVD) Runge-Kutta time discretization

To evolve $\bar{u}_j(t)$ in (2.1) for the finite volume WENO scheme or $u_j^{(l)}(t)$ in (2.11) for the DG method in time, we use the third order total variation diminishing (TVD) Runge-Kutta method in [14]. Explicitly, for the system of ODEs $u_t = L(u)$, the evolution from u^n to u^{n+1}

is obtained through

$$\begin{aligned} u^{(1)} &= u^n + \Delta t L(u^n, t^n) \\ u^{(2)} &= \frac{3}{4}u^n + \frac{1}{4}(u^{(1)} + \Delta t L(u^{(1)})) \\ u^{n+1} &= \frac{1}{3}u^n + \frac{2}{3}(u^{(2)} + \Delta t L(u^{(2)})). \end{aligned} \tag{2.12}$$

The details of its implementation can be found in [14].

3 Examples of scalar nonconvex conservation laws

3.1 Examples with good performance of high order schemes

In this subsection, we will give two examples of nonconvex conservation laws for which the high order numerical methods perform nicely and converge to the entropy solutions.

- **The Buckley-Leverett Equation.** This is a one-dimensional model problem for two-phase fluid flow in a porous medium with the application in oil-reservoir simulation. The conservation law is (1.1) with the flux function given by

$$f(u) = \frac{u^2}{u^2 + a(1-u)^2} \quad \text{where } a = \frac{1}{2}, \tag{3.1}$$

and the initial condition given by

$$u_0(x) = \begin{cases} 1, & \text{for } x < 0, \\ 0, & \text{for } x \geq 0. \end{cases} \tag{3.2}$$

Figure 3.1 shows the solution $u(x, t)$ of the Buckley-Leverett equation (1.1)-(3.1) with the initial condition (3.2) at the time $t = 2$. The exact solution is obtained by the convex-hull construction [8]. We observe that both the finite volume WENO scheme and the discontinuous Galerkin method with a WENO limiter approximate the exact solution very well in this example. We have computed this example using the discontinuous Galerkin method with a WENO limiter of orders of accuracy from 2 to 4 and have obtained similarly good solutions, even though only the second order result is plotted in Figure 3.1 to save space.

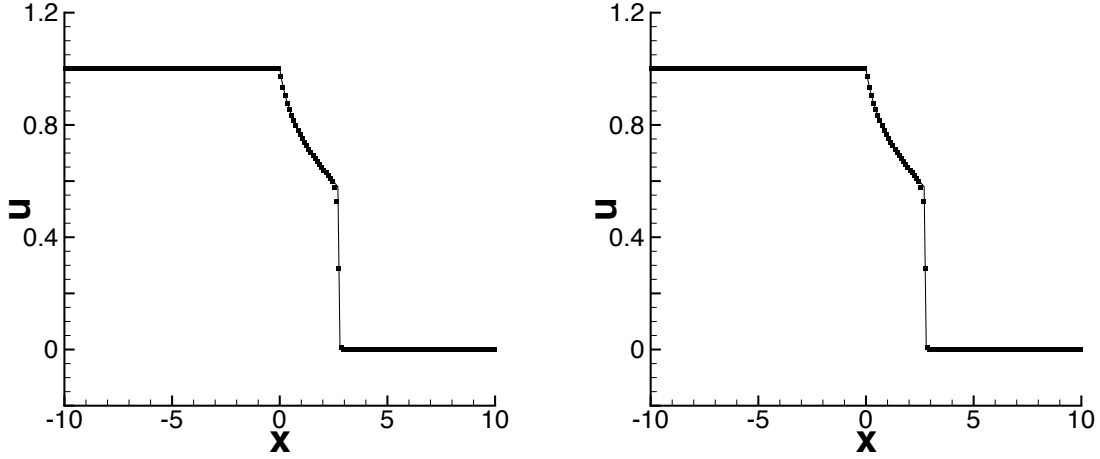


Figure 3.1: Solid lines: the exact solution of (1.1)-(3.1) with the initial condition (3.2) at the time $t = 2$; solid symbols: the numerical solution of the fifth order finite volume WENO scheme (left) and the second order discontinuous Galerkin method with WENO limiters (right). The uniform mesh size is $\Delta x = 0.1$.

- **Another example.** The following example is used in [7]. It is a Riemann problem for the scalar one-dimensional nonconvex conservation laws (1.1) with the flux function given by

$$f(u) = \begin{cases} \frac{u(1-u)}{4}, & \text{if } u < \frac{1}{2}, \\ \frac{1}{2}u^2 - \frac{1}{2}u + \frac{3}{16}, & \text{if } u \geq \frac{1}{2}, \end{cases} \quad (3.3)$$

and the initial condition given by

$$u_0(x) = \begin{cases} 0, & \text{for } x < 0, \\ 1, & \text{for } x \geq 0. \end{cases} \quad (3.4)$$

Figure 3.2 shows the solution $u(x, t)$ for the Riemann problem of (1.1)-(3.3) with the initial condition (3.4) at the time $t = 2$. The exact solution is obtained by the convex-hull construction. Again, we have computed this example using the DG method with a WENO limiter from second to fourth order accuracy and have obtained similarly good solutions, even though only the second order result is shown in Figure 3.2. The high order numerical methods are observed to approximate the exact solution very well for this example.

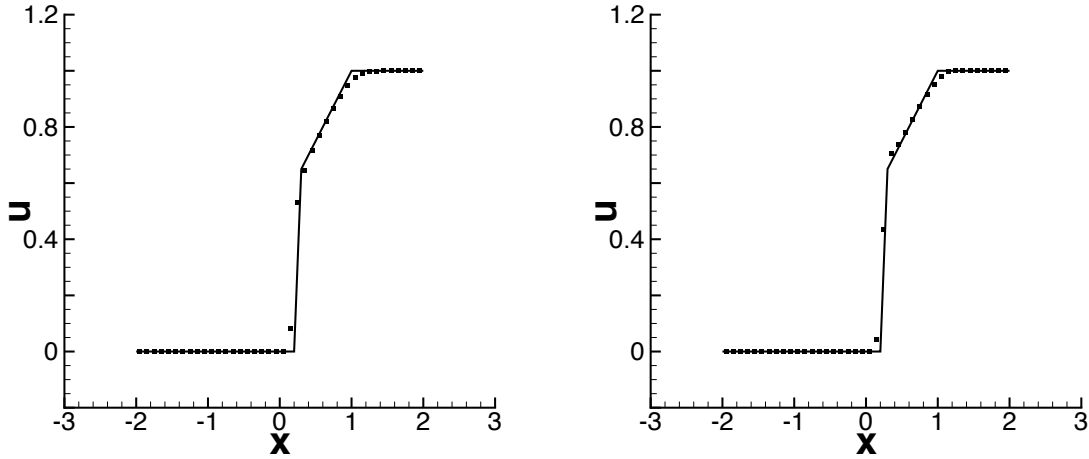


Figure 3.2: Solid lines: the exact solution of (1.1)-(3.3) with the initial condition (3.4) at the time $t = 2$; solid symbols: the numerical solution of the fifth order finite volume WENO scheme (left) and the second order discontinuous Galerkin method with WENO limiters (right). The uniform mesh size is $\Delta x = 0.1$.

3.2 An example of nonconvex conservation laws with poor performance of high order schemes

Despite the good performance of high order numerical methods in the examples demonstrated above, there are also examples for which the performance of high order numerical methods is poor. In this subsection, we will show a nonconvex conservation law, such that many high order numerical schemes do not converge to the unique entropy solution. Indeed, we will show in the following that the numerical solution of the second order finite volume MUSCL scheme, the second order DG method, and the high order Godunov type scheme with fifth order WENO reconstruction and the usual time step governed by the CFL condition, all with the Godunov flux (2.3), would stay stationary on the initial data for a specific sequence of meshes. On the other hand, the correct entropy solution for this case would develop a sequence of shocks and rarefaction waves.

Proposition 3.1. Consider the semi-discrete finite volume scheme with the second order MUSCL reconstruction (2.5) and the monotone Godunov flux (2.3), for solving (1.1) with

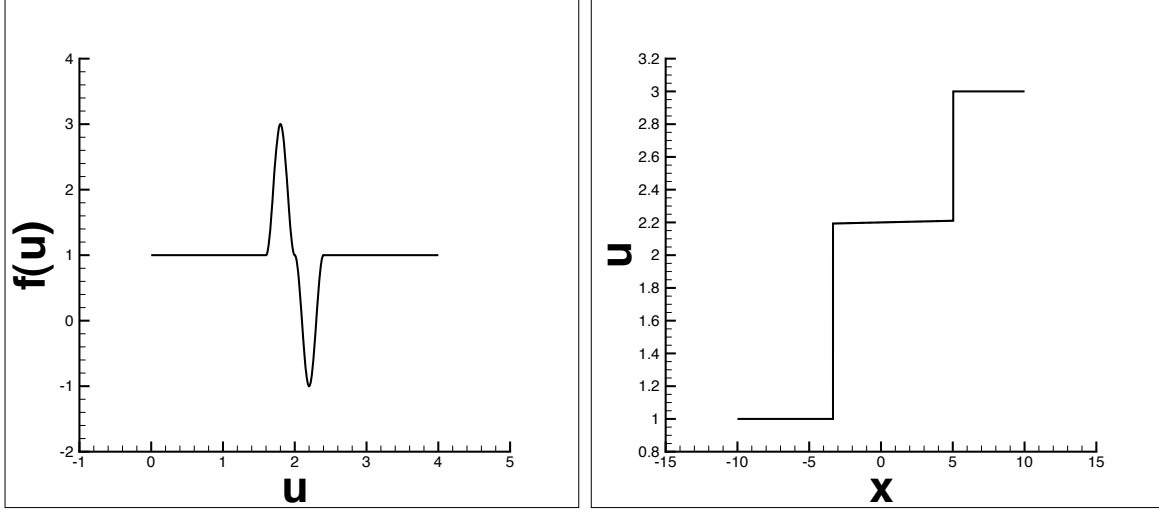


Figure 3.3: Left: the nonconvex flux function $f(u)$; Right: the exact solution of (1.1)-(3.5) with the initial condition (3.6) at the time $t = 2$.

the nonconvex flux $f(u)$ defined by

$$f(u) = \begin{cases} 1, & \text{if } u < 1.6 \\ \cos(5\pi(y - 1.8)) + 2.0, & \text{if } 1.6 \leq u < 2.0 \\ -\cos(5\pi(y - 2.2)), & \text{if } 2.0 \leq u < 2.4 \\ 1, & \text{if } u \geq 2.4 \end{cases} \quad (3.5)$$

(see the left panel of Figure 3.3) and the initial condition

$$u_0(x) = \begin{cases} 1, & \text{for } x < 0 \\ 3, & \text{for } x \geq 0 \end{cases} \quad (3.6)$$

The numerical solution stays stationary over the time evolution for a specific sequence of meshes. Therefore, the second order finite volume MUSCL scheme does not converge to the correct entropy solution in this case (the right panel of Figure 3.3).

Proof: In order to prove that the numerical solution stays stationary, it is sufficient to prove that the right hand side of (2.1) equals 0 for any j .

We first divide the computational interval into $N = (2m + 1)$ evenly spaced subintervals such that the origin 0 is located in the center of the $(m + 1)$ -th cell, i.e. $x_{m+1} = 0$. With such a specific sequence of meshes, and under the initial condition (3.6), the initial cell averages are given by

$$\bar{u}_j^0 = 1, \quad \text{for } j = 1, \dots, m; \quad \bar{u}_{m+1}^0 = 2; \quad \bar{u}_j^0 = 3, \quad \text{for } j = m + 2, \dots, N,$$

and the corresponding reconstructed point values by the MUSCL procedure (2.5) at the cell boundaries are

$$u_{j+\frac{1}{2}}^{\pm,0} = 1, \quad \text{for } j = 0, \dots, m-1; \quad u_{j+\frac{1}{2}}^{\pm,0} = 3, \quad \text{for } j = m+2, \dots, N;$$

$$u_{m+\frac{1}{2}}^{-,0} = 1, \quad u_{m+\frac{1}{2}}^{+,0} = 1.5, \quad u_{m+\frac{3}{2}}^{-,0} = 2.5, \quad u_{m+\frac{3}{2}}^{+,0} = 3.$$

If we use the monotone Godunov flux (2.3) as the numerical flux, then $\hat{f}_{j+\frac{1}{2}}^G = 1$ for all j , even for the flux at $x_{m+\frac{1}{2}}$ and $x_{m+\frac{3}{2}}$ where

$$\hat{f}_{m+\frac{1}{2}}^G = \hat{f}^G(u_{m+\frac{1}{2}}^-, u_{m+\frac{1}{2}}^+) = \hat{f}^G(1, 1.5) = \max_{u \in (1, 1.5)} f(u) = 1,$$

$$\hat{f}_{m+\frac{3}{2}}^G = \hat{f}^G(u_{m+\frac{3}{2}}^-, u_{m+\frac{3}{2}}^+) = \hat{f}^G(2.5, 3) = \min_{u \in (2.5, 3)} f(u) = 1.$$

Therefore, the right hand side of (2.1) equals 0 for all j . This implies that the cell averages \bar{u}_j , hence the numerical solution of the finite volume MUSCL scheme, stays stationary as (3.6) over time.

The correct entropy solution can be solved by the convex hull reconstruction. The entropy solution at the time $t = 2$ is plotted in the right panel of Figure 3.3. The discontinuity at the origin in the initial condition generates a shock, a rarefaction wave followed by another shock over time. Clearly the numerical solution of the finite volume MUSCL scheme fails to converge to the correct entropy solution in this case. Indeed, we can easily check that the stationary numerical solution is one of the weak solutions, but not the entropy solution, as it violates the entropy inequality for the convex entropies $U(u) = |u - c|$ with $c \in [2.0, 2.2]$. This completes the proof. ■

Proposition 3.2. Consider the semi-discrete DG method (2.11) for (1.1) with the nonconvex flux $f(u)$ defined by (3.5) and the initial condition (3.6). The numerical solution of the second order DG method with the Godunov flux (2.3) will stay stationary over time for a specific sequence of meshes. Therefore, the DG method could not converge to the correct entropy solution (the right panel of Figure 3.3).

Proof: Let the sequence of meshes be the same as that in the proof of Proposition 3.1 and consider the second order DG method with the solution space and test space to be the piecewise linear function $V_{\Delta x}^1$ as in (2.8). If we adopt a local orthogonal basis over I_j as $\{1, \xi_j\}$ with $\xi_j = \frac{x-x_j}{\Delta x_j}$, the semi-discrete DG method is formulated as finding $u^{\Delta x} = u_j^{(0)} + u_j^{(1)}\xi_j$ on I_j , such that

$$\frac{\partial}{\partial t} u_j^{(0)} = -\frac{1}{\Delta x_j} \left(\hat{f}_{j+\frac{1}{2}} - \hat{f}_{j-\frac{1}{2}} \right) \quad (3.7)$$

$$\frac{1}{12} \frac{\partial}{\partial t} u_j^{(1)} = \frac{1}{\Delta x_j} \left(\frac{1}{\Delta x_j} \int_{I_j} f(u^{\Delta x}) dx - \left(\frac{1}{2} \hat{f}_{j+\frac{1}{2}} + \frac{1}{2} \hat{f}_{j-\frac{1}{2}} \right) \right) \quad (3.8)$$

Initially, from (3.6), we have

$$u_j^{(0)} = \begin{cases} 1, & \text{for } j = 1, 2, \dots, m \\ 2, & \text{for } j = m+1 \\ 3, & \text{for } j = m+2, \dots, N \end{cases} \quad (3.9)$$

$$u_j^{(1)} = \begin{cases} 0, & \text{for } j = 1, 2, \dots, m \\ 3, & \text{for } j = m+1 \\ 0, & \text{for } j = m+2, \dots, N \end{cases} \quad (3.10)$$

By (2.3), it could be easily checked that the Godunov flux

$$\hat{f}_{j+\frac{1}{2}}^G = 1, \quad \forall j, \quad (3.11)$$

and

$$\frac{1}{\Delta x} \int_{I_j} f(u^{\Delta x}) dx = 1, \quad \forall j, \quad (3.12)$$

even for the flux at the boundaries of the $(m+1)$ -th cell. Therefore, for any j , the right hand sides of both (3.7) and (3.8) vanish. In other words, both the mean value and the slope of the numerical solution over each cell would stay stationary over time. Therefore, the numerical solution of the semi-discrete DG method with the Godunov flux stays stationary with respect to the initial condition (3.6) and could not converge to the correct entropy solution as shown in the right panel of Figure 3.3. This completes the proof. ■

Proposition 3.3. Consider the high order Godunov type scheme (2.7) with the fifth order WENO reconstruction (2.6), for solving (1.1) with the nonconvex flux function $f(u)$ defined

by (3.5) and the initial condition (3.6). The numerical solution stays stationary when the time step is small enough for a specific sequence of meshes. Numerical solution of this high order Godunov type scheme therefore could not converge to the correct entropy solution (the right panel of Figure 3.3).

Proof: The proof is similar to that in [18], and is thus omitted. ■

We have shown that the numerical solutions for (1.1)-(3.5) with the initial condition (3.6) would stay stationary for many high order schemes including the second order finite volume MUSCL scheme, the second order discontinuous Galerkin method and the fifth order Godunov type WENO scheme with the Godunov flux, which is the least dissipative among all monotone fluxes, for a specific sequence of meshes. The numerical solutions of these schemes with more dissipative fluxes, e.g. the Lax-Friedrichs flux, or with different meshes, however, may not necessarily be stationary. In the following, we compare the performance of different schemes with different types of numerical fluxes and different meshes for solving (1.1) with the flux $f(u)$ given by (3.5). We have performed extensive numerical experiments, but are presenting only a selected few to demonstrate the poor performance of the low order monotone schemes (slow convergence) and high order schemes (slow or no convergence).

1. Monotone scheme with the Lax-Friedrichs flux (the left panel of Figure 3.4) and with the Godunov flux (the right panel of Figure 3.4) for the initial data (3.6).
2. Monotone scheme with the Lax-Friedrichs flux (the left panel of Figure 3.5) and with the Godunov flux (the right panel of Figure 3.5) for the initial condition

$$u_0(x) = \begin{cases} 3, & \text{for } -1 \leq x < 0 \\ 1, & \text{for } 0 \leq x \leq 1 \end{cases} \quad (3.13)$$

and a periodic boundary condition.

3. Fifth order finite volume WENO scheme with the Lax-Friedrichs flux (the left panel of Figure 3.6) and with the Godunov flux (the right panel of Figure 3.6) for the initial data (3.6).

4. Discontinuous Galerkin method with WENO limiters (DG-WENO), with the Lax-Friedrichs flux (the left panels of Figure 3.7) and with the Godunov flux (the right panels of Figure 3.7) for the initial data (3.6).

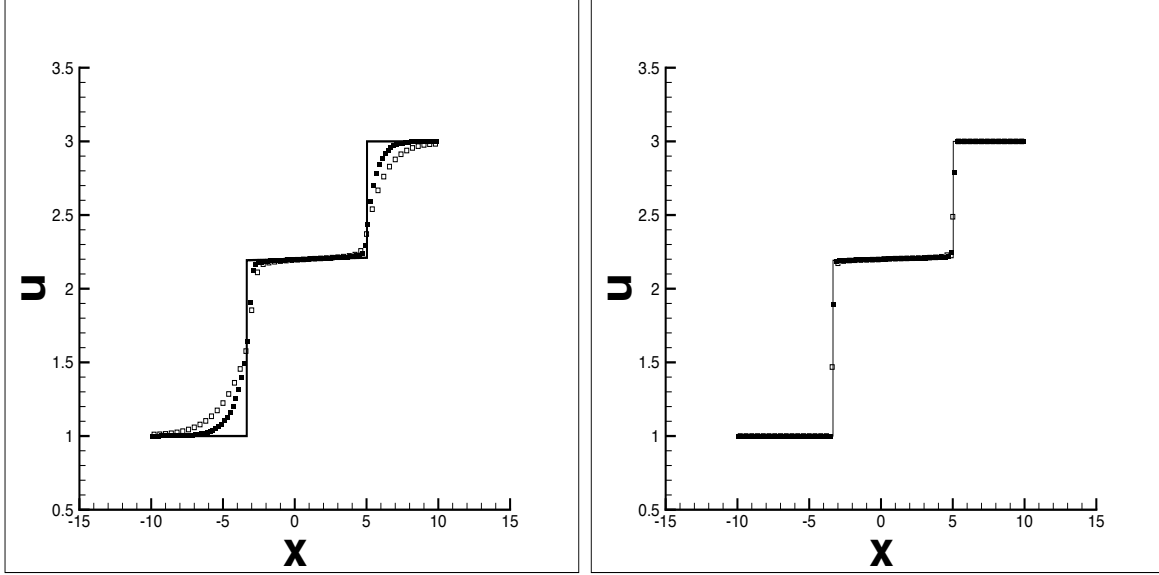


Figure 3.4: The numerical solution of the monotone scheme with the Lax-Friedrichs flux (left) and the Godunov flux (right) for the nonconvex scalar conservation law (1.1)-(3.5) with the initial condition (3.6) at $t = 2$ using $N = 50$ (unfilled square) and $N = 100$ (filled square) uniform cells.

From the demonstrated numerical results, we can make the following observations.

1. The first order monotone scheme with the Godunov flux has a much better performance than the one with the Lax-Friedrichs flux (see Figure 3.4). However, with a periodic boundary condition, after shocks and rarefaction waves interact with each other, the convergence is very slow even for the first order Godunov scheme (see Figure 3.5).
2. The fifth order finite volume WENO scheme with the Godunov flux might not converge to the correct entropy solution. The scheme with the Lax-Friedrichs flux seems to converge to the entropy solution with a slow convergence rate (the left panel of Figure 3.6), which might be related to the fact that the reconstruction of the solution at the rarefaction wave comes from neighboring cells and is not a good approximation when

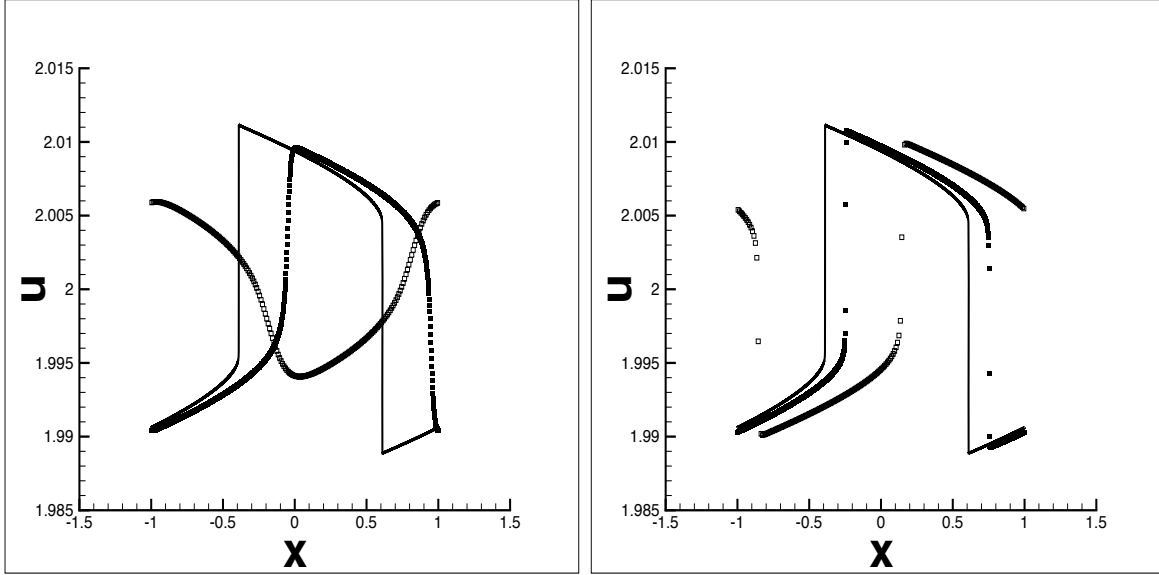


Figure 3.5: The numerical solution of the monotone scheme with the Lax-Friedrichs flux (left) and the Godunov flux (right) for the nonconvex scalar conservation law (1.1)-(3.5) with the initial condition (3.13) at $t = 2$ with a periodic boundary condition using $N = 200$ (unfilled square), $N = 1000$ (filled square) and $N = 36000$ (solid line) uniform cells.

the rarefaction wave is surrounded by two shocks at its early stage of development. Further numerical experiments on (1.1)-(3.5) with the initial condition (3.13) indicate that the finite volume WENO scheme with the Lax-Friedrichs flux could not converge to the entropy solution.

3. The DG scheme with WENO limiters might not converge to the correct entropy solution of (1.1). Different meshes, fluxes and solution spaces in the DG scheme will give different numerical results. The numerical solutions seem to converge to the correct entropy solution in some but not all cases.

3.3 Another nonconvex conservation law: $f(u) = \sin(u)$

In section 3.2, we have shown a nonconvex conservation law, with which the numerical solution of the high order schemes could not converge to the correct entropy solution. Indeed this is not the only example. We will show in the following another example of poor performance of high order numerical methods. Consider the Riemann problem of the nonconvex

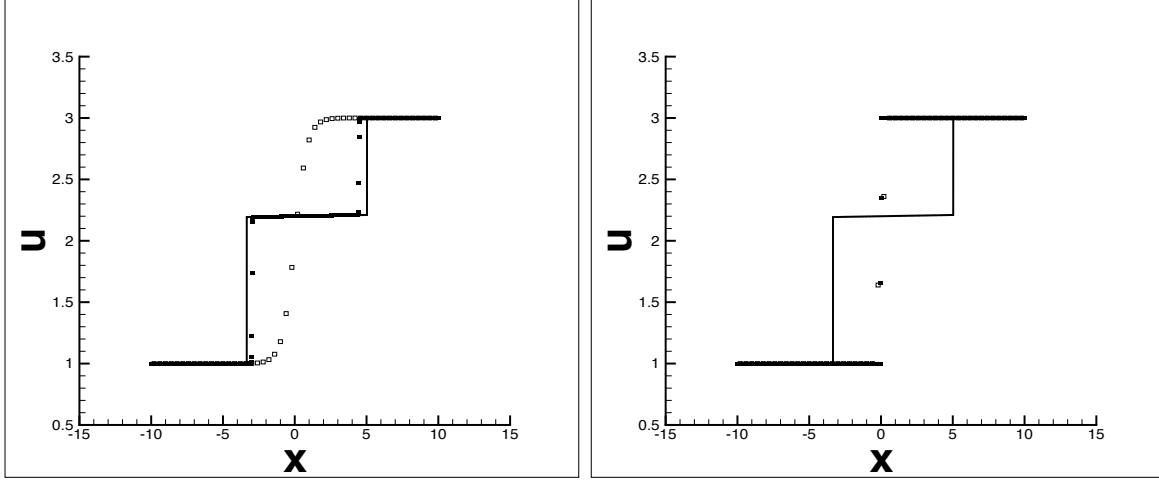


Figure 3.6: The numerical solution of the fifth order finite volume WENO scheme with the Lax-Friedrichs flux (left) and the Godunov flux (right) for the nonconvex scalar conservation law (1.1)-(3.5) with the initial condition (3.6) at $t = 2$ using $N = 50$ (unfilled square) and $N = 800$ (filled square) uniform cells.

conservation law (1.1) with the flux function

$$f(u) = \sin(u),$$

and the initial condition

$$u_0(x) = \begin{cases} \pi/64, & \text{if } x < 0, \\ 255\pi/64, & \text{if } x \geq 0. \end{cases} \quad (3.14)$$

It is shown, in Figure 3.8 for the high order finite volume schemes and in Figure 3.9 for the discontinuous Galerkin methods, that the numerical solution of these high order schemes would not always converge to the entropy solution. One of the rarefaction waves in the compound wave is sometimes missing in the solutions of these high order schemes.

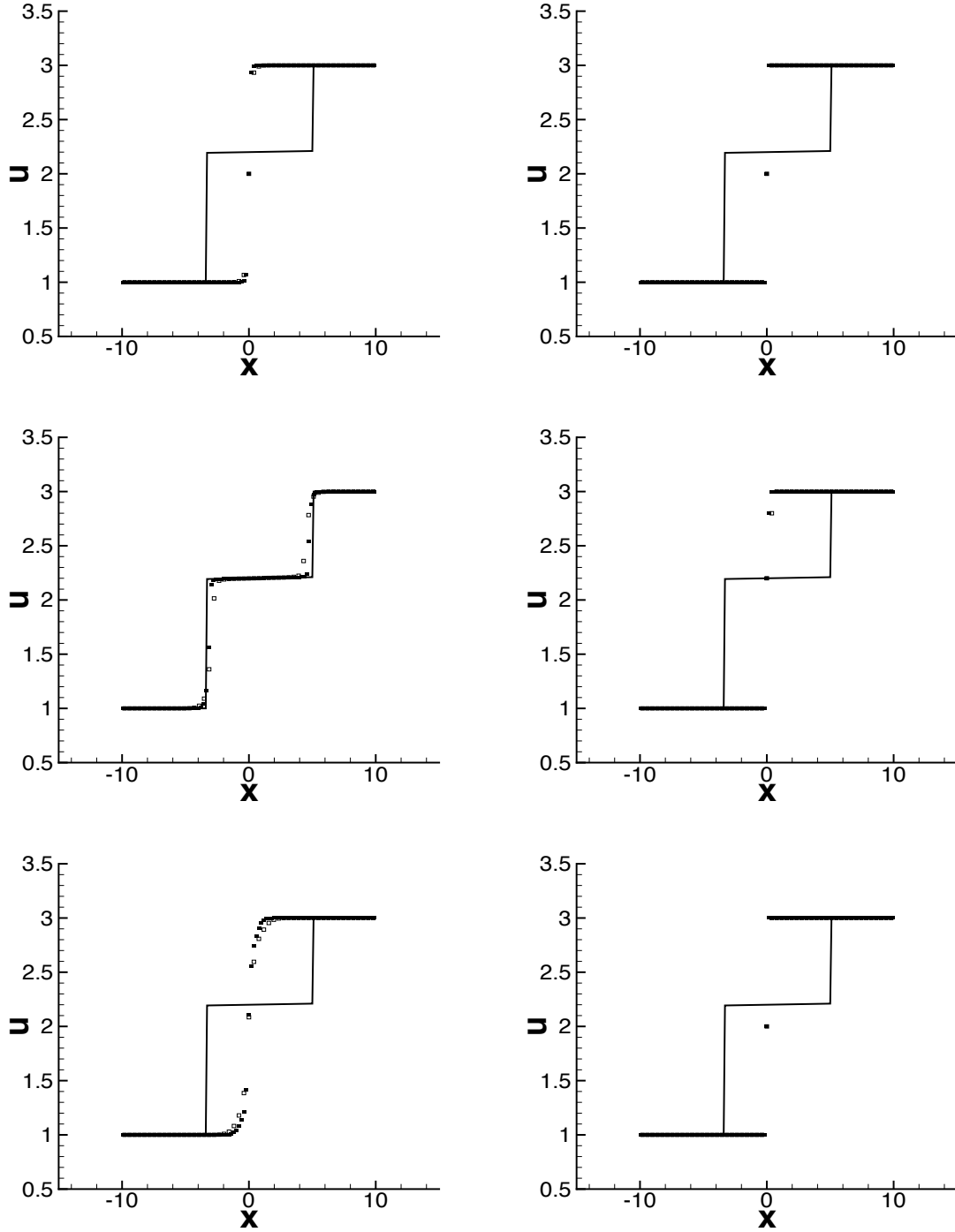


Figure 3.7: The numerical solution of the DG-WENO schemes at $t = 2$ for (1.1)-(3.5) with the initial condition (3.6) and the Lax-Friedrichs flux (left) and the Godunov flux (right) using $N = 51$ (unfilled square) and $N = 101$ (filled square) uniform cells. From top to bottom are figures for the second, third and fourth order schemes respectively.

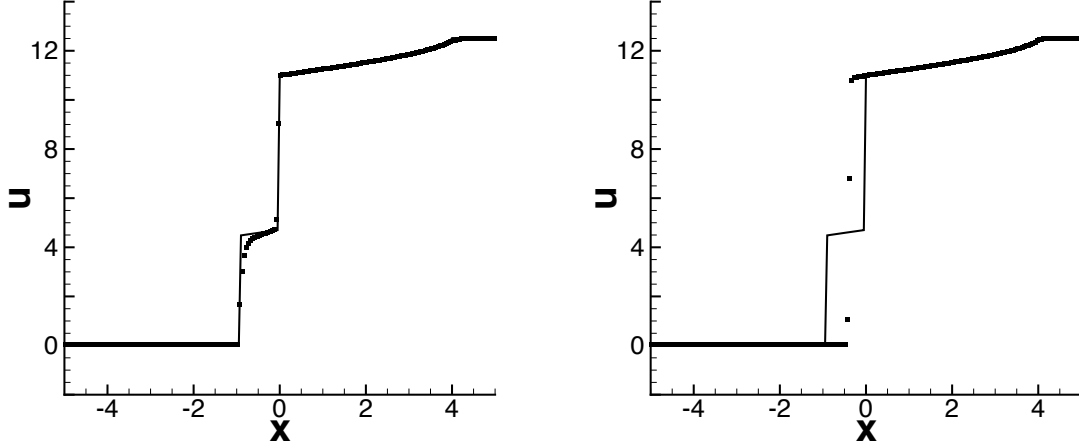


Figure 3.8: Solid lines: the exact solution of (1.1) with $f(u) = \sin(u)$ and the initial condition (3.14) at the time $t = 4$; solid symbols: the numerical solution of the second order MUSCL scheme (left), and the fifth order finite volume WENO scheme (right). The numerical flux is the Godunov flux. The mesh is uniform with $\Delta x = 0.05$.

4 First order monotone modification

In this section, we propose a first order monotone modification for high order numerical methods. The objective is to maintain high order accuracy in smooth regions and enforce convergence to the entropy solution for general nonconvex conservation laws. The maintenance of high order accuracy is achieved by a carefully designed discontinuity indicator [16].

4.1 Discontinuity indicator

In order to maintain the high order accuracy in smooth regions, we use the discontinuity indicator designed in [16]. Specifically, the discontinuity indicator ϕ_j is defined as

$$\phi_j = \frac{\beta_j}{\beta_j + \gamma_j} \quad (4.1)$$

where

$$\alpha_j = |\bar{u}_{j-1} - \bar{u}_j|^2 + \varepsilon, \quad \xi_j = |\bar{u}_{j+1} - \bar{u}_{j-1}|^2 + \varepsilon, \quad \beta_j = \frac{\xi_j}{\alpha_{j-1}} + \frac{\xi_j}{\alpha_{j+2}}, \quad \gamma_j = \frac{(u_{\max} - u_{\min})^2}{\alpha_j}.$$

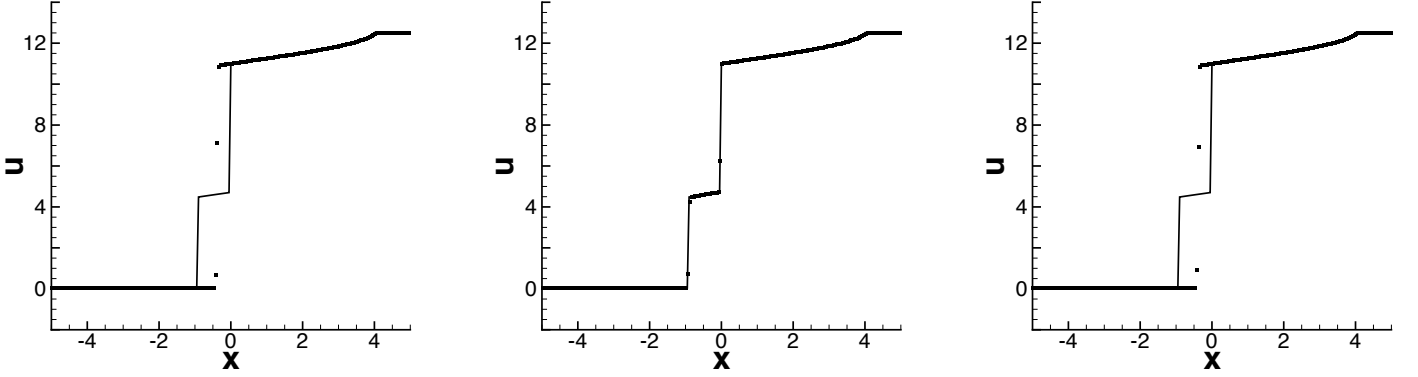


Figure 3.9: Solid lines: the exact solution of (1.1) with $f(u) = \sin(u)$ and the initial condition (3.14) at the time $t = 4$; solid symbols: the discontinuous Galerkin method with WENO limiters, of second order accuracy (left), third order accuracy (middle) and fourth order accuracy (right). The numerical flux is the Godunov flux. The mesh is uniform with $\Delta x = 0.05$.

Here \bar{u}_j refers to the cell average of the numerical solution on I_j in the finite volume scheme and the discontinuous Galerkin method, ε is a small positive number taken as 10^{-6} in the code, and u_{\max} and u_{\min} are the maximum and minimum values of \bar{u}_j over all cells. The discontinuity indicator ϕ_j has the property that

- $0 \leq \phi_j \leq 1$.
- ϕ_j is on the order of $O(\Delta x^2)$ in smooth regions.
- ϕ_j is close to $O(1)$ near a strong discontinuity.

4.2 Modification on the fifth order finite volume WENO scheme

In this section, we propose a first order modification to the fifth order finite volume WENO scheme. Recall from section 2.1 that the cell average \bar{u}_j in the finite volume WENO scheme is updated by

$$\frac{d\bar{u}_j}{dt} = -\frac{1}{\Delta x_j}(\hat{f}_{j+\frac{1}{2}} - \hat{f}_{j-\frac{1}{2}}), \quad (4.2)$$

in which the numerical flux $\hat{f}_{j+\frac{1}{2}} = \hat{f}(u_{j+\frac{1}{2}}^-, u_{j+\frac{1}{2}}^+)$, or more precisely, the reconstructed point values $u_{j+\frac{1}{2}}^\pm$ at the cell boundaries play an essential role. The modification proposed is based

on modifying $u_{j+\frac{1}{2}}^\pm$ at the cell boundaries. The scheme can be summarized as following, after a suitable initialization to obtain \bar{u}^0 .

1. Perform the WENO reconstruction.

At each cell interface, say $x_{j+\frac{1}{2}}$, reconstruct the point values $u_{j+\frac{1}{2}}^\pm$ using neighboring cell averages \bar{u}^n by the fifth order WENO reconstruction procedure described in section 2.1.

2. Identify the troubled cell boundary $x_{j+\frac{1}{2}}$.

Criterion I: A cell boundary $x_{j+\frac{1}{2}}$ is good, if $u_{j+\frac{1}{2}}^\pm$, \bar{u}_j and \bar{u}_{j+1} all fall into the same linear, convex or concave region of the flux function $f(u)$. Otherwise, it is defined to be a troubled cell boundary.

When the flux function $f(u)$ is nonconvex, one can divide its domain into several subregions, across each of which $f(u)$ is purely linear, convex or concave. For example, for $f(u)$ defined in (3.5), there are several linear regions, e.g. $[-\infty, 1.6]$, $[2.4, \infty]$, convex regions, e.g. $[1.6, 1.7]$, $[1.9, 2.0]$, $[2.1, 2.3]$, and concave regions, e.g. $[1.7, 1.9]$, $[2.0, 2.1]$, $[2.3, 2.4]$. Points are said to fall into the same region if all of them are contained in the same subregion.

3. At troubled cell boundaries, modify the numerical flux $\hat{f}_{j+\frac{1}{2}}$ with a discontinuity indicator.

Let $\hat{f}_{j+\frac{1}{2}} = \hat{f}(u_{j+\frac{1}{2}}^{m,-}, u_{j+\frac{1}{2}}^{m,+})$, where

$$u_{j+\frac{1}{2}}^{m,-} = (1 - \phi_j^2)u_{j+\frac{1}{2}}^- + \phi_j^2\bar{u}_j, \quad u_{j+\frac{1}{2}}^{m,+} = (1 - \phi_j^2)u_{j+\frac{1}{2}}^+ + \phi_j^2\bar{u}_{j+1}, \quad (4.3)$$

with ϕ_j defined by (4.1), if $x_{j+\frac{1}{2}}$ is a troubled cell boundary. Otherwise, at good cell boundaries, $u_{j+\frac{1}{2}}^{m,\pm} = u_{j+\frac{1}{2}}^\pm$.

4. Evolve the cell averages \bar{u}_j by (4.2).

Remark. When a troubled cell boundary is at a strong discontinuity, $\phi_j \sim 1$, hence $u_{j+\frac{1}{2}}^{m,-} \sim \bar{u}_j$ and $u_{j+\frac{1}{2}}^{m,+} \sim \bar{u}_{j+1}$, indicating a first order monotone scheme is taking the effect at a nonconvex discontinuity region. When a troubled cell boundary is in a smooth region, the modification is obtained with the magnitude at most of the size

$$\phi_j^2 \max \left(\left| u_j - u_{j+\frac{1}{2}}^- \right|, \left| u_{j+1} - u_{j+\frac{1}{2}}^+ \right| \right) \sim O(\Delta x^5),$$

hence it does not affect the fifth order accuracy of the scheme.

Numerical examples are given below to check the maintained order of accuracy for smooth solutions and convergence towards the entropy solution.

Example 4.1. The nonconvex conservation law

$$u_t + \left(\frac{u^3}{3} \right)_x = 0, \quad u_0(x) = \sin(\pi x). \quad (4.4)$$

Table 4.1 gives the L^1 errors and the corresponding orders of accuracy of the regular and modified finite volume WENO scheme. The L^1 errors of both schemes are comparable. Very little difference is observed.

Table 4.1: The L^1 errors and the corresponding orders of accuracy for the regular and modified finite volume WENO schemes with the Godunov flux for (4.4) at the time $t = 0.2$.

No. of points	regular		modified	
	L^1 error	order	L^1 error	order
100	2.128E-05		2.128E-05	
200	1.120E-06	4.25	1.120E-06	4.25
300	1.648E-07	4.73	1.648E-07	4.73
400	4.079E-08	4.85	4.079E-08	4.85
500	1.366E-08	4.90	1.366E-08	4.90

Example 4.2. The nonconvex conservation law (1.1) with $f(u) = \sin(u)$ and the initial condition (3.14). The solutions at the time $t = 4$ are plotted in the left panel of Figure 4.1. As shown, the numerical solutions of the modified scheme successfully converge to the correct entropy solution, with the development of the complex solution structure containing a shock, a rarefaction wave, followed by another shock and another rarefaction wave.

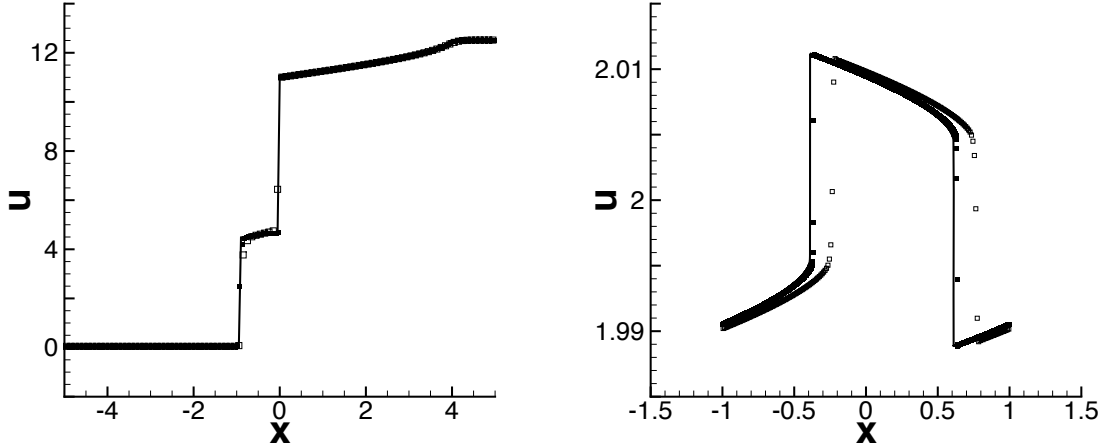


Figure 4.1: Left figure: Example 4.2. Solid lines: the exact solution at time $t = 4$; solid symbols: the numerical solution of the modified fifth order finite volume WENO scheme with the uniform mesh size $\Delta x = 0.1$ (unfilled squares), $\Delta x = 0.05$ (solid symbols). Right figure: Example 4.3. Solid lines: the reference solution (computed by the first order monotone Godunov scheme with $N = 36000$ points) at time $t = 2$; symbols: the numerical solution of the modified fifth order finite volume WENO scheme with $N = 200$ (unfilled square) and $N = 1000$ (filled square) uniform cells. The numerical flux in both figures is the Godunov flux.

Example 4.3. The nonconvex conservation law (1.1) with $f(u)$ given by (3.5), the initial condition (3.13) and a periodic boundary condition. As shown in the right panel of Figure 4.1, the numerical solution of the modified scheme converges to the correct entropy solution, with much faster convergence rate when compared to the first order monotone scheme (Figure 3.5). We also test our modified scheme by further refining the numerical meshes. Convergence to the entropy solution is observed.

4.3 Modification on the discontinuous Galerkin methods

In this subsection, we propose a first order modification to the high order discontinuous Galerkin methods. Recalling from section 2.2, the piecewise polynomial over each cell I_j is updated by its moments $u_j^{(l)}(t)$ as defined in (2.10) through (2.11). To modify high order DG methods, we make the following two observations:

1. Only the numerical flux $\hat{f}_{j+\frac{1}{2}}$, or more precisely, the left and right limits of discontinuous

solution $u_{j+\frac{1}{2}}^-$ and $u_{j+\frac{1}{2}}^+$ at the cell interface are involved in updating the cell average $u_j^{(0)}$.

2. The whole polynomial over I_j is involved in updating the higher order moments $u_j^{(l)}$ for $l \geq 1$ through the integration term on the right hand side of (2.11).

Based on these two observations, a monotone modification for $(k+1)$ -th ($k \geq 1$) order DG methods with WENO limiters is designed as follows. After a suitable initialization,

$$u_j^{(l)} = \frac{1}{a_l} \int_{I_j} u(x, 0) v_l^{(j)}(x) dx, \quad l = 0, 1, 2, \dots, k.$$

1. Apply the WENO limiters in the oscillatory troubled cells.

The oscillatory troubled cells refer to those cells where oscillations at discontinuities might occur in high order DG methods. We refer to [12] for the details of identifying such oscillatory troubled cells and reconstructing high order polynomials there by the WENO procedure.

2. Identify the nonconvex troubled cells.

Criterion II: A cell I_j is called a good cell, if the numerical solution $u^{\Delta x}$ in the cells I_{j-1} , I_j and I_{j+1} falls into the same linear, convex or concave region of the flux function $f(u)$. Otherwise, it is defined to be a nonconvex troubled cell.

3. Evolve the polynomial solution.

- If a cell I_j is good, then evolve the polynomial function $u^{\Delta x}|_{I_j}$ by the regular DG method through (2.11).
- Otherwise, evolve the cell average $u_j^{(0)}$ only by

$$\frac{du_j^{(0)}}{dt} = -\frac{1}{\Delta x_j} (\hat{f}_{j+\frac{1}{2}} - \hat{f}_{j-\frac{1}{2}}), \quad (4.5)$$

where the numerical flux $\hat{f}_{j+\frac{1}{2}} = \hat{f}(u_{j+\frac{1}{2}}^{m,-}, u_{j+\frac{1}{2}}^{m,+})$ with

$$u_{j+\frac{1}{2}}^{m,-} = (1 - \phi_j^2) u_{j+\frac{1}{2}}^- + \phi_j^2 u_j^{(0)}, \quad u_{j+\frac{1}{2}}^{m,+} = (1 - \phi_j^2) u_{j+\frac{1}{2}}^+ + \phi_j^2 u_{j+1}^{(0)},$$

with ϕ_j defined by (4.1) at the troubled cell boundaries as defined via Criteria I in section 4.2, and $u_{j+\frac{1}{2}}^{m,\pm} = u_{j+\frac{1}{2}}^{\pm}$ at good cell boundaries.

4. Reconstruct the polynomials in the troubled cells.

For a troubled cell I_j , where only the cell average is updated, the polynomial is reconstructed from neighboring cell averages in a WENO fashion, as in [12].

Example 4.4. The nonconvex conservation law (4.4). Tables 4.2 and 4.3 give the L^1 errors and the corresponding orders of accuracy of the regular DG-WENO methods and the modified DG-WENO methods respectively. The tables show comparable L^1 errors.

Table 4.2: The L^1 errors and the corresponding orders of accuracy for the regular DG-WENO method with the Godunov flux for (4.4) at the time $t = 0.2$.

No. of points	$k = 1$		$k = 2$		$k = 3$	
	L^1 error	order	L^1 error	order	L^1 error	order
30	5.207E-03		7.655E-04		3.679E-04	
60	1.230E-03	2.08	4.889E-05	3.97	5.403E-06	6.09
90	5.365E-04	2.05	1.265E-05	3.33	6.844E-07	5.10
120	2.862E-04	2.18	5.122E-06	3.14	2.045E-07	4.20
150	1.648E-04	2.47	2.608E-06	3.02	8.341E-08	4.02

Table 4.3: The L^1 errors and the corresponding orders of accuracy for the modified DG-WENO method with the Godunov flux for (4.4) at the time $t = 0.2$.

No. of points	$k = 1$		$k = 2$		$k = 3$	
	L^1 error	order	L^1 error	order	L^1 error	order
30	2.313E-03		1.146E-03		6.951E-04	
60	1.242E-03	4.40	4.924E-05	4.54	5.714E-06	6.93
90	5.382E-04	2.06	1.264E-05	3.35	7.044E-07	5.16
120	2.866E-04	2.19	5.120E-06	3.14	2.048E-07	4.29
150	1.649E-04	2.48	2.608E-06	3.02	8.291E-08	4.05

Example 4.5. The nonconvex conservation law (1.1) with $f(u) = \sin(u)$ and the initial condition (3.14). Its solution at the time $t = 4$ of the second and fourth order DG-WENO

methods are plotted in Figure 4.2. As shown, the numerical solutions of the modified schemes successfully converge to the correct entropy solution.

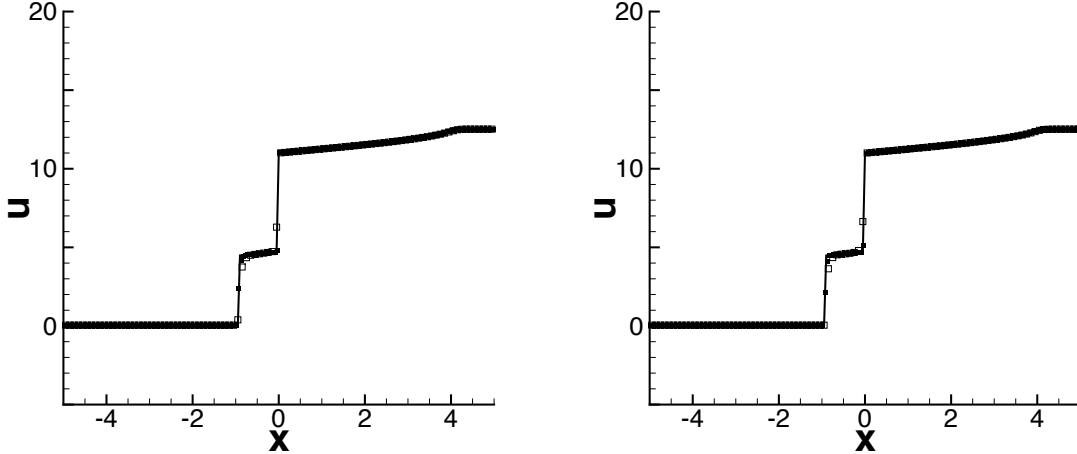


Figure 4.2: Solid lines: the exact solution of (1.1) with (3.14) at the time $t = 4$; solid symbols: the modified discontinuous Galerkin method with WENO limiters, of second order accuracy (left) and fourth order accuracy (right). The numerical flux is the Godunov flux. The uniform mesh sizes are $\Delta x = 0.1$ (unfilled squares) and $\Delta x = 0.05$ (solid symbols), respectively.

Example 4.6. The nonconvex conservation law (1.1) with $f(u)$ defined in (3.5), the initial condition (3.13) and a periodic boundary condition. As shown in Figure 4.3, the numerical solutions of the modified schemes converge to the correct entropy solution with much faster convergence rate when compared with the first order monotone scheme. We also test our modified scheme by further refining the numerical mesh. Convergence to the entropy solution is observed.

5 Second order modification with an entropic projection

A MUSCL type method with an entropic projection, enjoying the cell entropy inequality for all convex entropy functions, is proposed in [1]. This entropy satisfying property for all convex entropy functions is very attractive in the design of high order numerical methods

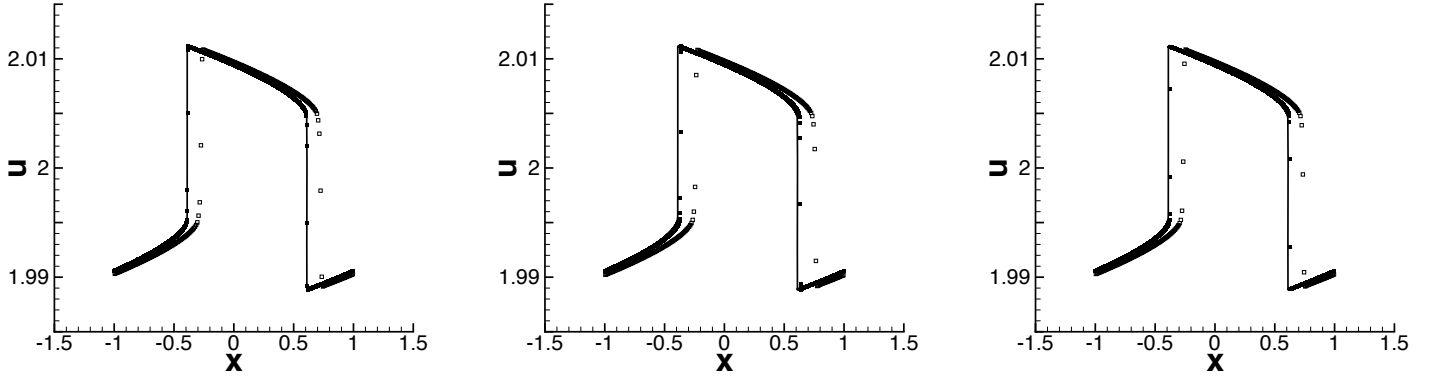


Figure 4.3: Solid lines: the reference solution obtained by the first order monotone Godunov scheme with $N = 36000$ grid points for (1.1) with (3.5), the initial condition (3.13) and a periodic boundary condition at the time $t = 2$. Symbols: the modified discontinuous Galerkin method with WENO limiters, of second order accuracy (left), third order accuracy (middle) and fourth order accuracy (right) with $N = 200$ (unfilled squares) and $N = 1000$ (solid squares) uniform cells. The numerical flux is the Godunov flux.

for general nonconvex conservation laws. Based on the idea of this entropic projection, we propose a second order modification for the high order schemes.

5.1 Review of the MUSCL method satisfying all the numerical entropy inequalities

The scheme in [1] uses piecewise linear functions as the solution space. Specifically, the numerical solution at time level n can be written as $u^n = \bar{u}_j^n + s_j^n \xi_j$ with $\xi_j = \frac{x-x_j}{\Delta x_j}$ over the cell I_j . It consists of two steps to evolve from u^n to u^{n+1} .

1. *Exact evolution* ($T_{\Delta t}$): Evolve (1.1) exactly for a time step Δt , to obtain a solution \tilde{u}^{n+1} , which in general is not a piecewise linear function anymore.
2. *An entropic projection* (P^1): Find a second order approximation to \tilde{u}^{n+1} by a piecewise linear function u^{n+1} , satisfying

$$\int_{I_j} U(u^{n+1}(x)) dx \leq \int_{I_j} U(\tilde{u}^{n+1}(x)) dx, \quad \forall j \quad (5.1)$$

for all convex entropy functions $U(u)$. Second order reconstruction satisfying (5.1) can be obtained by setting the cell average as

$$\bar{u}_j^{n+1} = \frac{1}{\Delta x_j} \int_{I_j} \tilde{u}^{n+1} \quad (5.2)$$

and the slope as

$$s_j^{n+1} = D\tilde{u}^{n+1} |_{I_j} = \text{minmod}_{I_j} \zeta(y) \quad (5.3)$$

where

$$\zeta(y) = \frac{2}{\Delta x_j} \left(\frac{1}{x_{j+\frac{1}{2}} - y} \int_y^{x_{j+\frac{1}{2}}} \tilde{u}^{n+1}(x) dx - \frac{1}{y - x_{j-\frac{1}{2}}} \int_{x_{j-\frac{1}{2}}}^y \tilde{u}^{n+1}(x) dx \right). \quad (5.4)$$

The minmod function of $g(x)$ on the interval (a, b) is defined as

$$\text{minmod}_{(a,b)} g(x) = \begin{cases} 0, & \text{if } \exists y_1, y_2 \in (a, b), \quad s.t. \quad g(y_1)g(y_2) \leq 0, \\ \min_{(a,b)} g(y), & \text{if } g(y) > 0, \quad \forall y \in (a, b), \\ \max_{(a,b)} g(y), & \text{if } g(y) < 0, \quad \forall y \in (a, b). \end{cases} \quad (5.5)$$

In summary, the scheme can be written out in the following abstract form

$$u^{n+1} = P^1 \circ T_{\Delta t}(u^n) \doteq Q^1(\Delta t)(u^n). \quad (5.6)$$

It enjoys the following convergence theorem as proved in [1]. Comparing with the high order Godunov type schemes (2.7) which may fail to satisfy at least some entropy conditions [18], the entropic projection (P^1), especially, the reconstruction of the slope s_j^{n+1} in (5.3), is crucial to ensure convergence towards the entropy solution.

Theorem 5.1 [1]. Let $T = n\Delta t$, $u(\cdot, T)$ be the exact entropy solution to (1.1) with the initial data $u_0 \in L^1 \cap BV(\mathcal{R})$, $f_\infty = \max_{u \in [\min u_0, \max u_0]} f'(u)$, then there exists a constant C , such that

$$\|Q^1(\Delta t)^n u^0 - u(\cdot, T)\|_{L^1} \leq C(f_\infty \sqrt{T\Delta t} + \Delta x \sqrt{T/\Delta t}). \quad (5.7)$$

Therefore, the second order MUSCL scheme with the entropic projection (5.6) converges to the unique entropy solution.

5.2 Second order schemes with the entropic projection

In this subsection, the entropic projection (P^1), or more explicitly, the reconstruction of the slope s_j^{n+1} in (5.3), is used to design a second order method for general nonconvex conservation laws. With a suitable initialization to obtain a piecewise linear function, $\bar{u}_j^0 + s_j^0 \xi_j$ with $\xi_j = \frac{x-x_j}{\Delta x_j}$, the scheme consists of the following steps in each time step evolution.

1. Identify nonconvex troubled cells, for which we refer to Criterion II in section 4.3 for the details.
2. Update \bar{u}_j^{n+1} for the good cells.

If a cell I_j is good, evolve \bar{u}_j^n by the regular finite volume method through (4.2), where $\hat{f}_{j+\frac{1}{2}} = \hat{f}(u_{j+\frac{1}{2}}^-, u_{j+\frac{1}{2}}^+)$ with $u_{j+\frac{1}{2}}^-$ and $u_{j+\frac{1}{2}}^+$ being the left and right limits of the numerical solution at the cell interface.

3. Update \bar{u}_j^{n+1} and s_j^{n+1} in nonconvex troubled cells.

If a cell I_j is a nonconvex troubled cell, update $u^{n+1}|_{I_j}$ by (5.2) and (5.3), where $\tilde{u}^{n+1}|_{I_j}$ is approximated by a first order refined mesh evolution. Specifically, a first order monotone scheme is used to numerically evolve (1.1) with the initial condition

$$\bar{u}_l^n + s_l^n \xi_l, \text{ for } x \in I_l, \quad l=j-1, j, j+1 \quad (5.8)$$

and a periodic boundary condition on $I_{j-1} \cup I_j \cup I_{j+1}$ for time Δt . We remark that periodic boundary condition is allowed here as the information outside the domain, $I_{j-1} \cup I_j \cup I_{j+1}$, would not affect the solution on I_j after time Δt , which is restricted by the CFL condition. Let I_j be uniformly discretized by

$$I_j = \cup_{m=1}^N [y_{m-\frac{1}{2}}, y_{m+\frac{1}{2}}], \quad \delta x = y_{m+\frac{1}{2}} - y_{m-\frac{1}{2}} = \Delta x/N,$$

then $\tilde{u}^{n+1}|_{I_j}$ is approximated by a piecewise constant function sitting on the refined numerical mesh with the truncation error $\sim \mathcal{O}(\delta x) = \mathcal{O}(\Delta x^2)$. (5.3) is numerically

implemented by finding y among the (finitely many) refined cell boundaries $y_{m+\frac{1}{2}}$ ($m = 0, \dots, N$) that minimizes $\zeta(y)$ as defined in (5.4).

4. Update s_j^{n+1} in the good cells.

In the good cells, reconstruct the slope s_j^{n+1} in the MUSCL fashion from neighboring cell averages.

Remark. The implementation of the entropic projection proposed above is very computational expensive and impractical. An efficient implementation for specific equations, for example for the Burgers equation with the flux function $f(u) = \frac{u^2}{2}$ is available in [1]. For general nonconvex flux functions, an efficient implementation for the entropic projection is nontrivial and is worth a further investigation.

In the following, we provide numerical examples of the proposed second order scheme with the entropic projection.

Example 5.1. The nonconvex conservation law (4.4). Table 5.1 gives the L^1 errors and the corresponding orders of accuracy for the regular second order finite volume scheme with the MUSCL reconstruction and the proposed scheme with the entropic projection. The table shows comparable L^1 errors and second order accuracy as expected.

Table 5.1: The L^1 errors and the corresponding orders of accuracy for the regular second order finite volume scheme with the MUSCL reconstruction and the proposed scheme with the entropic projection for (4.4) at the time $t = 0.2$.

No. of points	MUSCL		entropic projection	
	L^1 error	order	L^1 error	order
60	3.198E-03		3.202E-03	
120	8.863E-04	1.85	8.865E-04	1.85
180	4.129E-04	1.88	4.129E-04	1.88
240	2.394E-04	1.90	2.394E-04	1.90
300	1.548E-04	1.95	1.548E-04	1.95
360	1.095E-04	1.90	1.095E-04	1.90

Example 5.2. The nonconvex conservation laws (1.1) with $f(u) = \sin(u)$ and the initial condition (3.14). The solutions at the time $t = 4$ are plotted in the left panel of Figure 5.1. As shown, the numerical solution of the scheme with the entropic projection successfully converges to the correct entropy solution, with better resolution of the rarefaction wave when compared with the regular MUSCL reconstruction (the left panel of Figure 3.8).

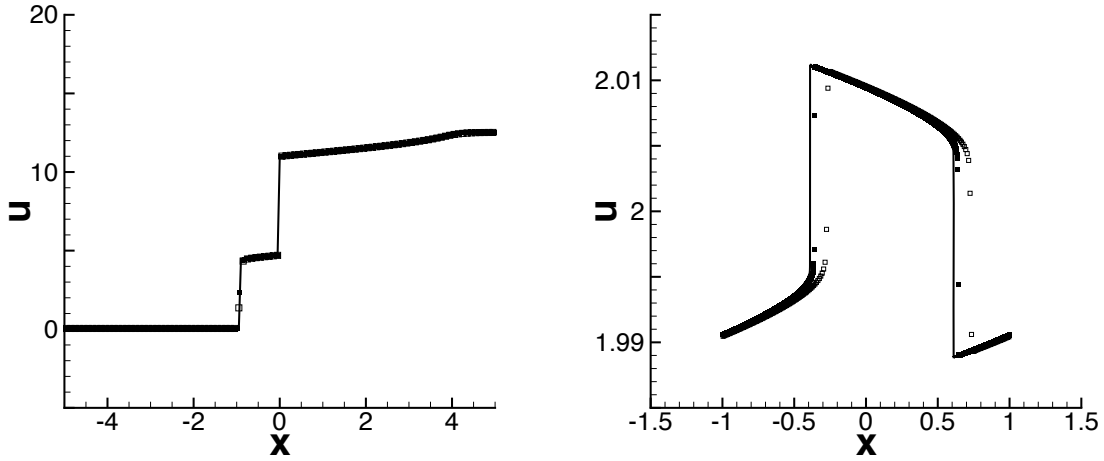


Figure 5.1: Left figure: the solid line is the exact solution of (1.1) with (3.14) at the time $t = 4$, while the solid symbols are the numerical solution of the second order finite volume scheme with the entropic projection with $\Delta x = 0.1$ (unfilled squares), $\Delta x = 0.05$ (solid symbols). Right figure: the solid line is the reference solution (obtained with a first order monotone Godunov scheme with $N = 36000$ grid points) at the time $t = 2$, while the symbols are the numerical solution of the second order scheme with the entropic projection with $N = 200$ (unfilled squares) and $N = 1000$ (solid symbols) uniform cells. The numerical flux in both figures is the Godunov flux.

Example 5.3. The nonconvex conservation law (1.1) with $f(u)$ defined by (3.5), the initial condition (3.13) and a periodic boundary condition. As shown in the right panel of Figure 5.1, the numerical solution of the second order scheme with the entropic projection converges to the correct entropy solution, with much faster convergence rate when compared with the first order monotone scheme (Figure 3.5).

5.3 Second order modification to the fifth order finite volume WENO schemes

In this subsection, the second order method just designed is used as a building block to modify the fifth order finite volume WENO scheme. The modification follows a similar line as the first order monotone modification described in section 4.2. The procedure is outlined as following.

At each time step evolution, we would like to update $u_j = \{\bar{u}_j, u_{j\mp\frac{1}{2}}^\pm, u_j^l, u_j^r\}$ over the cell I_j . At the initial stage, $u_{j\mp\frac{1}{2}}^\pm$ is obtained by the WENO reconstruction from \bar{u} . u_j^l and u_j^r refer to approximations to the left and right boundaries of I_j . $u_j^l = u_{j-\frac{1}{2}}^+$ and $u_j^r = u_{j+\frac{1}{2}}^-$.

1. Identify the troubled cell boundaries, for which we refer to Criterion I in section 4.2 for the details.
2. Modify the numerical flux $\hat{f}_{j+\frac{1}{2}}$ with a discontinuity indicator.

Specifically, let $\hat{f}_{j+\frac{1}{2}} = \hat{f}(u_{j+\frac{1}{2}}^{m,-}, u_{j+\frac{1}{2}}^{m,+})$, where

$$u_{j+\frac{1}{2}}^{m,-} = (1 - \phi_j^2)u_{j+\frac{1}{2}}^- + \phi_j^2 u_j^r, \quad u_{j+\frac{1}{2}}^{m,+} = (1 - \phi_j^2)u_{j+\frac{1}{2}}^+ + \phi_j^2 u_{j+1}^l, \quad (5.9)$$

with ϕ_j defined by (4.1) at the troubled cell boundary. At good cell boundaries, $u_{j+\frac{1}{2}}^{m,\pm} = u_{j+\frac{1}{2}}^\pm$.

3. Identify nonconvex troubled cells.

Criterion II': A cell I_j is called a good cell, if $u^m = \{\bar{u}_m, u_{m\mp\frac{1}{2}}^\pm, u_m^l, u_m^r\}$ with $m = j-1, j, j+1$, fall into the same linear, convex or concave region of the flux function $f(u)$. Otherwise, it is defined to be a nonconvex troubled cell.

4. Update u_j^l and u_j^r for a nonconvex troubled cell I_j .

Perform a first order refined mesh evolution. Specifically, the first order monotone scheme is used to numerically evolve (1.1) with the initial condition (5.8) where

$$s_m^n = 2\min\text{mod}(u_m^r - \bar{u}_m, \bar{u}_m - u_m^l), \quad m = j-1, j, j+1$$

and a periodic boundary condition to obtain $\tilde{u}^{n+1}|_{I_j}$, the details of this step is given in section 5.2. \tilde{u}^{n+1} is then approximated by $\overline{\tilde{u}_j^{n+1}} + s_j^{n+1}\xi_j$ with $\overline{\tilde{u}_j^{n+1}}$ obtained from (5.2) and s_j^{n+1} from (5.3).

$$u_j^{l,n+1} = \overline{\tilde{u}_j^{n+1}} - \frac{1}{2}s_j^{n+1}, \quad u_j^{r,n+1} = \overline{\tilde{u}_j^{n+1}} + \frac{1}{2}s_j^{n+1}.$$

5. Update the cell averages \bar{u}^{n+1} by (4.2).
6. Update $u_{j\pm\frac{1}{2}}^\pm$ by the WENO reconstruction procedure.
7. For a good cell I_j , update u_j^l and u_j^r by setting $u_j^l = u_{j-\frac{1}{2}}^+$ and $u_j^r = u_{j+\frac{1}{2}}^-$.

Remark. Comparing with the monotone modification of high order schemes, there are two additional pieces of information in each time step evolution, namely u_j^l and u_j^r . They are second order approximations to the left and right boundaries of a troubled cell I_j and are used in (5.9) to modify the numerical flux.

In the following, we provide numerical examples of the modified fifth order finite volume scheme with the second order entropic projection.

Example 5.4. The nonconvex conservation law (4.4). Table 5.2 shows comparable L^1 errors and the corresponding orders of accuracy for the regular fifth order finite volume scheme and the modified one with the second order entropic projection.

Table 5.2: The L^1 errors and the corresponding orders of accuracy for the regular fifth order finite volume WENO scheme and the modified one with the second order entropic projection for (4.4) at the time $t = 0.2$. The numerical flux is the Godunov flux.

No. of points	regular		modified	
	L^1 error	order	L^1 error	order
100	2.128E-05		2.128E-05	
200	1.120E-06	4.25	1.120E-06	4.25
300	1.648E-07	4.73	1.648E-07	4.73
400	4.079E-08	4.85	4.079E-08	4.85
500	1.366E-08	4.90	1.366E-08	4.90

Example 5.5. The nonconvex conservation law (1.1) with $f(u) = \sin(u)$ and the initial condition (3.14). The solutions at time $t = 4$ are plotted in the left panel of Figure 5.2. As shown, the numerical solution of the modified fifth order finite volume scheme with the entropic projection successfully converges to the correct entropy solution.

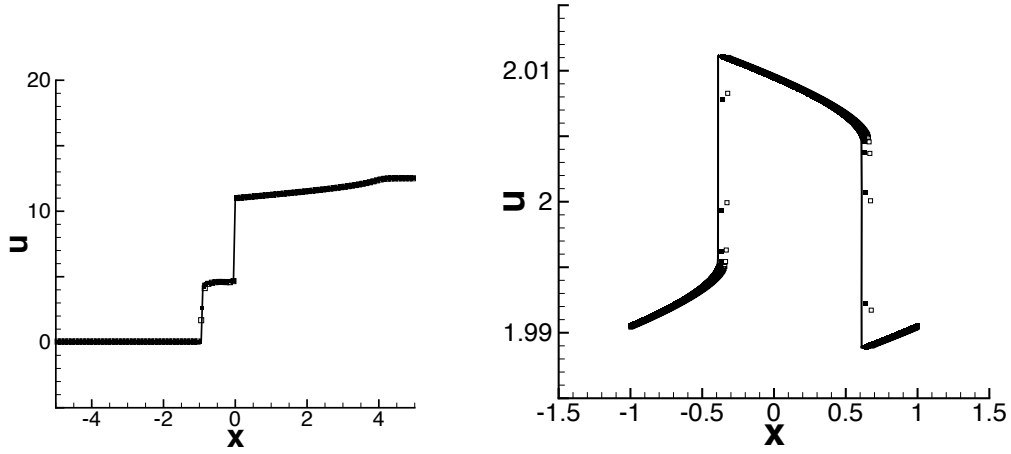


Figure 5.2: Left: Example 5.5. The solid line is the exact solution of (1.1) with (3.14) at the time $t = 4$, while the solid symbols are the numerical solution of the modified fifth order finite volume scheme with the entropic projection. The mesh size $\Delta x = 0.1$ (unfilled squares) and $\Delta x = 0.05$ (solid symbols). Right: Example 5.6. Solid lines: the reference solution obtained from the first order monotone Godunov scheme with $N = 36000$ grid points at the time $t = 2$; symbols: the numerical solution of the modified fifth order finite volume WENO scheme with the entropic projection with $N = 200$ (unfilled square) and $N = 400$ (filled square) uniform cells. The numerical flux in both figures is the Godunov flux.

Example 5.6. The nonconvex conservation law (1.1) with $f(u)$ defined by (3.5), the initial condition (3.13) and a periodic boundary condition. As shown in the right panel of Figure 5.2, the numerical solution of the fifth order finite volume WENO scheme with the second order entropic projection approximates the correct entropy solution very well with relatively coarse meshes, when compared with the first order modified high order schemes (the right panel of Figure 4.1).

5.4 Second order modification to the high order discontinuous Galerkin methods

In this subsection, the second order entropic projection is used as a building block to modify high order discontinuous Galerkin methods. The modification follows a similar line as the first order monotone modification presented in section 4.3. The procedure for a $(k + 1)$ -th order discontinuous Galerkin method is outlined as following.

At each time step evolution, we would like to update $u_j = \{u_j^{(0)}, \dots, u_j^{(k)}, u_j^l, u_j^r\}$ over the cell I_j . At the initial stage, $u_j^{(l)}$ is obtained by (2.10) and u_j^l and u_j^r refer to the point values at the left and right boundaries of the cell I_j . The scheme consists of the following steps in each time step evolution.

1. Apply the WENO limiters in the oscillatory troubled cells as described in section 4.3.
2. Identify nonconvex troubled cells I_j as described in Criterion II in section 4.3.
3. Identify nonconvex troubled cell boundaries as described in Criterion I in section 4.2.
4. Modify the numerical flux $\hat{f}_{j+\frac{1}{2}}$ with the discontinuity indicator.

Specifically, let $\hat{f}_{j+\frac{1}{2}} = \hat{f}(u_{j+\frac{1}{2}}^{m,-}, u_{j+\frac{1}{2}}^{m,+})$, where $u_{j+\frac{1}{2}}^{m,\pm}$ is computed from (5.9) at a troubled cell boundary. At good cell boundaries, $u_{j+\frac{1}{2}}^{m,\pm} = u_{j+\frac{1}{2}}^{\pm}$.

5. For good cells, update $u_j^{(l)}$ ($l = 0, \dots, k$) by the regular discontinuous Galerkin method and compute u_j^l and u_j^r from $u_j^{(l)}$ ($l = 0, \dots, k$).
6. For nonconvex troubled cells, update $u_j^{(0)}$ by (4.5) and update the remaining moments $u_j^{(l)}$ with $l \geq 1$ in a WENO fashion as in [12].
7. For nonconvex troubled cells I_j , update u_j^l and u_j^r as described in section 5.3.

In the following, we provide numerical examples of the modified high order discontinuous Galerkin methods with the second order entropic projection.

Example 5.7. The nonconvex conservation law (4.4). Table 5.3 gives the L^1 errors and the corresponding orders of accuracy for the modified DG-WENO scheme with the entropic projection. The L^1 errors of the modified DG-WENO method are comparable to those of the regular DG-WENO method shown in Table 4.2.

Table 5.3: The L^1 errors and the corresponding orders of accuracy for the modified DG-WENO method with the entropic projection at the time $t = 0.2$. The numerical flux is the Godunov flux.

No. of points	$k = 1$		$k = 2$		$k = 3$	
	L^1 error	order	L^1 error	order	L^1 error	order
30	5.313E-03		1.146E-04		6.951E-04	
60	1.244E-03	2.09	4.924E-05	4.54	5.714E-06	6.93
90	5.382E-04	2.06	1.264E-05	3.35	7.044E-07	5.16
120	2.866E-04	2.19	5.120E-06	3.14	2.048E-07	4.29
150	1.649E-04	2.47	2.608E-06	3.02	8.291E-08	4.05

Example 5.8. The nonconvex conservation law (1.1) with $f(u) = \sin(u)$ and the initial condition (3.14). The solutions at the time $t = 4$ are plotted in Figure 5.3. As shown, the numerical solution of the modified high order discontinuous Galerkin method with the entropic projection successfully converges to the correct entropy solution.

Example 5.9. The nonconvex conservation law (1.1) with $f(u)$ defined by (3.5), the initial condition (3.13) and a periodic boundary condition. As shown in Figure 5.4, the high order discontinuous Galerkin method with the second order entropic projection approximates the correct entropy solution very well with relatively coarse meshes. When comparing with the first order modified high order discontinuous Galerkin method (see Figure 4.3), the performance of the scheme has been greatly improved.

6 Concluding Remarks

We have investigated the performance of high order numerical methods for general one dimensional scalar nonconvex conservation laws, emphasizing convergence to the discontinuous

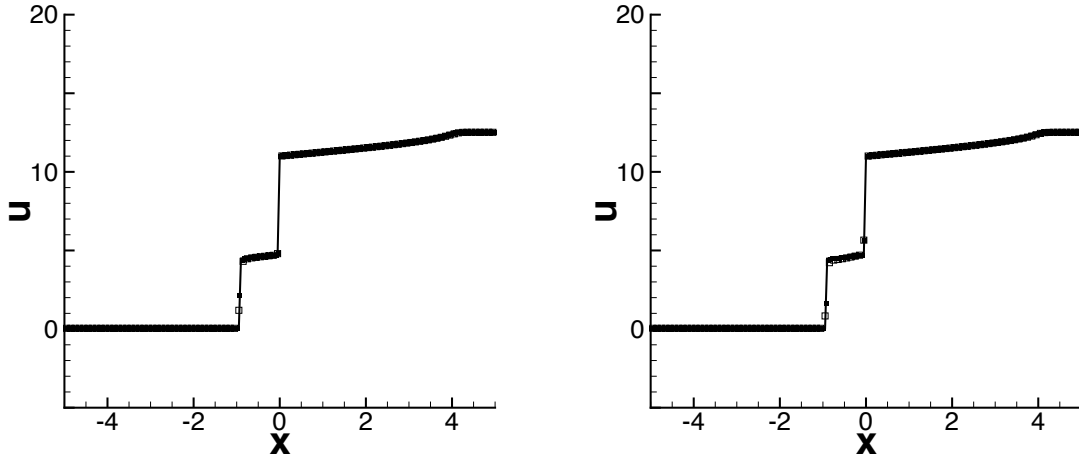


Figure 5.3: The solid line is the exact solution of (1.1) with (3.14) at the time $t = 4$, while the solid symbols are the numerical solution of the modified second order (left) and fourth order (right) discontinuous Galerkin method with the entropic projection. The uniform mesh sizes are $\Delta x = 0.1$ (unfilled squares) and $\Delta x = 0.05$ (solid symbols), respectively.

entropy solutions. It is observed that high order finite volume WENO and discontinuous Galerkin schemes may fail to converge to the entropy solutions for some difficult test cases. A first order modification based on first order monotone schemes and a second order modification based on an entropic projection are designed for high order finite volume WENO and discontinuous Galerkin methods to maintain high order accuracy in smooth regions and to enforce convergence to the entropy solution. Numerical examples are shown to demonstrate the quality of the proposed schemes. Future work will include more efficient implementation of the second order entropic projection, and a generalization of the current approach to multi-dimensional scalar problems and to systems.

References

- [1] F. Bouchut, CH. Bourdarias and B. Perthame, *A MUSCL method satisfying all the numerical entropy inequalities*, Mathematics of Computation, 65 (1996), pp.1438-1461.
- [2] B. Cockburn and C.-W. Shu, *TVB Runge-Kutta local projection discontinuous Galerkin finite element method for conservation laws II: General framework*, Mathematics of

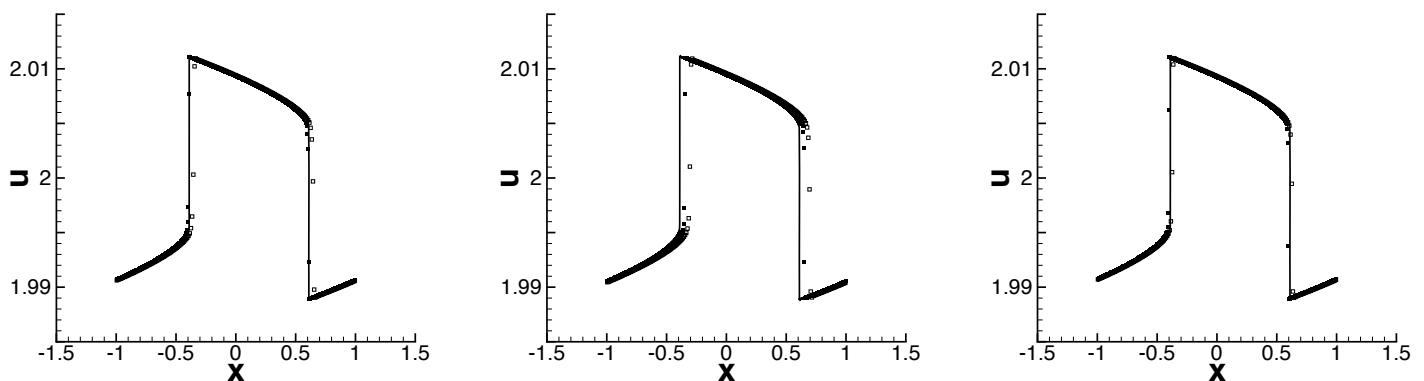


Figure 5.4: The solid line is the exact solution of (1.1) with (3.14) at the time $t = 2$, while the symbols are the numerical solution of the modified second order (left), third order (middle) and fourth order (right) discontinuous Galerkin method with the entropic projection with $N = 200$ (unfilled squares) and $N = 400$ (solid squares) uniform cells.

Computation, 52 (1989), pp.411-435.

- [3] M.G. Crandall and A. Majda, *Monotone difference approximations for scalar conservation laws*, Mathematics of Computation, 34 (1980), pp.1-21.
- [4] A. Harten, *High resolution schemes for hyperbolic conservation laws*, Journal of Computational Physics, 49 (1983), pp.357-393.
- [5] G.-S. Jiang and C.-W. Shu, *On cell entropy inequality for discontinuous Galerkin methods*, Mathematics of Computation, 62 (1994), pp.531-538.
- [6] G.-S. Jiang and C.-W. Shu, *Efficient implementation of weighted ENO schemes*, Journal of Computational Physics, 126 (1996), pp.202-228.
- [7] A. Kurganov, G. Petrova and B. Popov, *Adaptive semi-discrete central-upwind schemes for nonconvex hyperbolic conservation laws*, SIAM Journal on Scientific Computing, to appear.
- [8] R. LeVeque, *Numerical Methods for Conservation Laws*, Birkhauser Verlag, Basel, Switzerland, 1992.

- [9] X.-D. Liu, S. Osher and T. Chan, *Weighted essentially non-oscillatory schemes*, Journal of Computational Physics, 115 (1994), pp.200-212.
- [10] S. Osher and E. Tadmor, *On the convergence of the difference approximations to scalar conservation laws*, Mathematics of Computation, 50 (1988), pp.19-51.
- [11] J.-M. Qiu and C.-W. Shu, *Convergence of Godunov-type schemes for scalar conservation laws under large time steps*, SIAM Journal on Numerical Analysis, submitted.
- [12] J.-X. Qiu and C.-W. Shu, *Runge-Kutta discontinuous Galerkin method using WENO limiters*, SIAM Journal on Scientific Computing, 26 (2005), pp.907-929.
- [13] J. Shi, C. Hu and C.-W. Shu, *A technique of treating negative weights in WENO schemes*, Journal of Computational Physics, 175 (2002), pp.108-127.
- [14] C.-W. Shu and S. Osher, *Efficient implementation of essentially non-oscillatory shock capturing schemes*, Journal of Computational Physics, 77 (1988), pp.439-471.
- [15] B. van Leer, *Towards the ultimate conservative difference scheme V. A second order sequel to Godunov's method*, Journal of Computational Physics, 32 (1979), pp.101-136.
- [16] Z. Xu and C.-W. Shu, *Anti-diffusive finite difference WENO methods for shallow water with transport of pollutant*, Journal of Computational Mathematics, 24 (2006), pp.239-251.
- [17] H. Yang, *On wavewise entropy inequality for high-resolution schemes II: fully discrete MUSCL schemes with exact evolution in small time*, SIAM Journal on Numerical Analysis, 36 (1998), pp.1-31.
- [18] H. Yang, *Convergence of Godunov type schemes*, Applied Mathematics Letters, 9 (1996), pp.63-67.